JOURNAL OF GUIDANCE, CONTROL, AND DYNAMICS
Vol. 18, No. 3, May–June 1995

Robust Multirate Eigenstructure Assignment with Flight Control Application

J. E. Piou*
Binghamton University, Binghamton, New York 13902
and
K. M. Sobel†
City College of New York, New York, New York 10031

A recent result for multirate state feedback with fast and slow feedback loops is extended to output feedback. This multirate feedback structure is combined with eigenstructure assignment to design a lateral stability augmentation system operating at 50 Hz and a bank angle autopilot operating at 10 Hz for the linearized dynamics of the L-1011 aircraft. A new sufficient condition for robust stability of the multirate system in the presence of linear time-invariant continuous-time structured state-space uncertainty is proposed. A multiobjective optimization is used with both eigenstructure assignment and robustness objectives. A hybrid simulation of the continuous aircraft dynamics demonstrates that the robust multirate eigenstructure assignment flight control system exhibits excellent decoupling between the yaw and roll dynamics.

Introduction

MULTIRATE eigenstructure assignment was considered by Patel and Patton[1] by using the multi-input fixed-output (MIFO) rate configuration of Araki and Hagiwara.[2] However, the design of Ref. 1 is characterized by poor intersampling behavior. Later, Patel et al.[3] improved the intersampling behavior of MIFO eigenstructure assignment by using a numerical optimization that optimizes a performance index that penalizes gain magnitude and eigenvector assignment.

Huang[4] proposes an alternative multirate configuration that includes one loop with the states sampled at a fast rate and a second loop with the states sampled at a slower rate. The multirate controller has a set of fast gains, a set of slow gains, and a set of cross-coupling gains from the slow control to the fast control. This type of multirate aircraft flight control system is more typical than the MIFO configuration. Mason and Berg[5] use an implementation similar to Huang's,[4] but their mathematical representation is different because their model requires the inputs and outputs at N separate sampling times.

Huang's[4] design uses the linear quadratic regulator solution and hence requires full state feedback. Mason and Berg[5] use an optimization-based synthesis that does not incorporate robustness specifications into the design. Therefore, it is of interest to develop an output feedback multirate design methodology that incorporates specifications on robustness, damping/settling time (eigenvalues), and mode decoupling (eigenvectors). In this paper, we first extend Huang's[4] multirate state feedback results to output feedback for the case where the slow rate is an integer multiple of the fast rate. Then, we extend Piou and Sobel's[6] sufficient condition for robust stability to Huang's[4] multirate digital control system configuration.

The new results are used to design a multirate constant-gain output feedback eigenstructure assignment controller for the linearized lateral dynamics of the L-1011 aircraft described by Andry et al.[7] The controller consists of an inner stability augmentation system (SAS) loop operating at 50 Hz and an outer bank angle autopilot loop operating at 10 Hz. The SAS loop uses washed-out yaw rate, roll rate, and sideslip angle feedback whereas the autopilot loop uses bank angle feedback. This configuration is chosen based upon the assumption that the bank angle is obtained from the inertial navigation computer, which operates at a slower rate than the air data and flight control computers.

The first eigenstructure assignment design uses an orthogonal projection in which desired eigenvalues and eigenvectors are chosen to achieve specifications on damping, settling time, and mode decoupling. Then, the subroutine "attgoal" from the MATLAB™ Optimization Toolbox is used to compute a multiobjective controller with objectives on both the eigenstructure and robustness of the closed-loop system.

Time responses are obtained by using a SIMULINK™ hybrid simulation in which the aircraft is represented by continuous-time dynamics and the controller is represented by a multirate digital system. The time responses of both the orthogonal projection and robust multiobjective designs exhibit excellent intersampling behavior to an initial sideslip angle both with the autopilot on and with the autopilot off. In addition, excellent tracking of a step bank angle command with very little coupling to washed-out yaw rate is achieved when the autopilot is on.

Multirate Output Feedback

Consider the multirate system, which consists of a continuous-time plant and a digital controller, as shown in Fig. 1. This configuration was considered by Huang[4] using state feedback and is extended here to include output feedback. The fast and slow sampling rates are denoted by T_f and T_s, respectively. We assume that $T_s/T_f = m$, where m is an integer. We also assume that all control signals are held constant between transition times by zero-order holds and that all samplers are synchronized at the start. The fast and slow control signals are denoted by q_k and r_j, respectively. Here the index j is incremented every m cycles of the index k.

The continuous-time plant dynamics are described by

$$\dot{x}(t) = Ax(t) + Bu(t) \tag{1}$$

$$y(t) = Cx(t) \tag{2}$$

The outputs of the plant are divided into two groups $y_f(t)$ and $y_s(t)$, which denote the outputs sampled at the fast and slow rates, respectively. Mathematically,

$$y(t) = \begin{bmatrix} y_f(t) \\ y_s(t) \end{bmatrix} \tag{3}$$

Received April 18, 1994; presented as Paper 94-3542 at the AIAA Guidance, Navigation, and Control Conference, Scottsdale, AZ, Aug. 1–3, 1994; revision received Oct. 19, 1994; accepted for publication Nov. 10, 1994.

*Assistant Professor, Department of Electrical Engineering. Member AIAA.
†Professor, Department of Electrical Engineering. Associate Fellow AIAA.

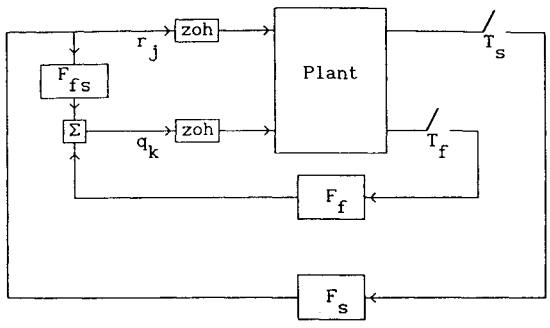

Fig. 1 Multirate feedback configuration.

where

$$y_f(t) = C_f x_f(t) \tag{4}$$

$$y_s(t) = C_s x_s(t) \tag{5}$$

and where $x_f(t)$ and $x_s(t)$ are the states at the fast and slow sampling times, respectively. Note that the state is not accessible so that $x_f(t)$ and $x_s(t)$ are only used for the mathematical development. Since the samplers are assumed to be synchronized, we have

$$x_{f_{k+m}} = x_{s_{j+1}} \tag{6}$$

If the system is discretized at the fast rate T_f, then Eqs. (1) and (2) become

$$x_{f_{k+1}} = \phi_f x_{f_k} + \Gamma_f q_k + \Gamma_{fs} r_j \tag{7}$$

$$y_{f_k} = C_f x_{f_k} \tag{8}$$

where

$$\phi_f = \exp(AT_f) \tag{9}$$

$$\Gamma_f = \int_0^{T_f} \exp(A\tau) B_f \, d\tau \tag{10}$$

$$\Gamma_{fs} = \int_0^{T_f} \exp(A\tau) B_s \, d\tau \tag{11}$$

where B_f and B_s are the columns of B corresponding to the control signals that are to be computed at the fast and slow rates, respectively. It is allowed that $B_f = B_s$ such that the inputs to the continuous-time plant are combinations of signals from both the fast and slow controllers.

To compute the fast gain F_f and the cross gain F_{fs}, we augment the discretized plant of Eq. (7) with $r_{k+1} = r_k$. This last equation is obtained by noting that the outputs of the slow controller are constant (except for the transitions) between the samples of the fast controller. Thus, we obtain

$$\begin{bmatrix} x_{f_{k+1}} \\ r_{k+1} \end{bmatrix} = \begin{bmatrix} \phi_f & \Gamma_{fs} \\ 0 & I \end{bmatrix} \begin{bmatrix} x_{f_k} \\ r_k \end{bmatrix} + \begin{bmatrix} \Gamma_f \\ 0 \end{bmatrix} q_k \tag{12}$$

We note that the modes corresponding to the r_k subsystem of Eq. (12) are uncontrollable. The fast control signal, which is computed by using Eq. (12), is given by

$$q_k = [F_f \quad F_{fs}] \begin{bmatrix} y_{f_k} \\ r_j \end{bmatrix} \tag{13}$$

If the slow control loop is open, then the system is described by the closed-loop fast dynamics. Substitute Eq. (13) into Eq. (7) with $r_j = 0$ to obtain

$$x_{f_{k+1}} = (\phi_f + \Gamma_f F_f C_f) x_{f_k} \tag{14}$$

Next, in order to compute the slow gain F_s, we need to obtain the dynamics that are referenced to the slow sampling rate. We substitute Eq. (13) into the fast dynamics of Eq. (7) and use Eq. (4) to obtain

$$x_{f_{k+1}} = (\phi_f + \Gamma_f F_f C_f) x_{f_k} + (\Gamma_{fs} + \Gamma_f F_{fs}) r_j \tag{15}$$

Advancing the time to $t = k + m$ in Eq. (15) yields

$$x_{f_{k+m}} = (\phi_f + \Gamma_f F_f C_f)^m x_{f_k} + \sum_{i=1}^{m} (\phi_f + \Gamma_f F_f C_f)^{m-i} (\Gamma_{fs} + \Gamma_f F_{fs}) r_j \tag{16}$$

Note that $x_{f_k} = x_{s_j}, \ldots, x_{f_{k+m}} = x_{s_{j+1}}, \ldots$ because the systems are synchronized at time $t = k$. Therefore, we may redefine the indices in Eq. (16) in terms of j and replace $x_{f_{k+m}}$ with $x_{s_{j+1}}$ to obtain

$$x_{s_{j+1}} = (\phi_f + \Gamma_f F_f C_f)^m x_{s_j} + \sum_{i=1}^{m} (\phi_f + \Gamma_f F_f C_f)^{m-i} (\Gamma_{fs} + \Gamma_f F_{fs}) r_j \tag{17}$$

The slow control signal, which is computed by using Eq. (17), is given by

$$r_j = F_s y_{s_j} \tag{18}$$

Finally, substitute Eq. (18) into Eq. (17) and use Eq. (5) to obtain the closed-loop system dynamics at the slow rate, which are described by

$$x_{s_{j+1}} = \left[(\phi_f + \Gamma_f F_f C_f)^m + \sum_{i=1}^{m} (\phi_f + \Gamma_f F_f C_f)^{m-i} \times (\Gamma_{fs} + \Gamma_f F_{fs}) F_s C_s \right] x_{s_j} \tag{19}$$

Robustness Results

Suppose that the continuous-time dynamics described by Eq. (1) are subject to uncertainty in the entries of A and B such that

$$\dot{x}(t) = Ax(t) + dA\, x(t) + Bu(t) + dB\, u(t)$$

$$y(t) = Cx(t)$$

Due to the partition of the system into slow and fast rates, the dynamics can be represented by

$$\dot{x}(t) = Ax(t) + dA\, x(t) + B_f q(t) + B_s r(t) + dB_f\, q(t) + dB_s\, r(t)$$

$$y(t) = Cx(t) \tag{20}$$

If the system is discretized at the fast rate of $1/T_f$, then

$$x_{f_{k+1}} = \exp[(A + dA)T_f] x_{f_k} + \int_0^{T_f} \exp[(A + dA)\tau](B_f + dB_f) q_k \, d\tau + \int_0^{T_f} \exp[(A + dA)\tau](B_s + dB_s) r_j \, d\tau \tag{21}$$

Let

$$d\phi_f = \exp[(A + dA)T_f] - \exp(AT_f) \tag{22}$$

$$d\Gamma_f = \int_0^{T_f} \exp[(A + dA)\tau](B_f + dB_f) \, d\tau - \int_f^{T_f} \exp(A\tau) B_f \, d\tau \tag{23}$$

$$d\Gamma_{fs} = \int_0^{T_f} \exp[(A + dA)\tau](B_f + dB_f)\,d\tau - \int_0^{T_f} \exp(A\tau)B_f\,d\tau \quad (24)$$

Then Eq. (21) can be written as

$$x_{f_{k+1}} = (\phi_f + d\phi_f)x_{f_k} + (\Gamma_f + d\Gamma_f)q_k + (\Gamma_{fs} + d\Gamma_{fs})r_j \quad (25)$$

Substitute the controller defined by Eq. (13) into Eq. (25) to obtain

$$x_{f_{k+1}} = (\phi_f + \Gamma_f F_f C_f)x_{f_k} + (d\phi_f + d\Gamma_f F_f C_f)x_{f_k} + (\Gamma_{fs} + \Gamma_f F_{fs})r_j + (d\Gamma_{fs} + d\Gamma_f F_{fs})r_j \quad (26)$$

Continue to advance the time until $t = k + m$ to obtain

$$x_{f_{k+m}} = [(\phi_f + \Gamma_f F_f C_f) + (d\phi_f + d\Gamma_f F_f C_f)]^m x_{f_k} + \sum_{i=1}^{m}[(\phi_f + \Gamma_f F_f C_f) + (d\phi_f + d\Gamma_f F_f C_f)]^{m-i} \times [(\Gamma_{fs} + \Gamma_f F_{fs}) + (d\Gamma_{fs} + d\Gamma_f F_{fs})]r_j \quad (27)$$

$$x_{f_{k+m}} = (\phi_f + \Gamma_f F_f C_f)^m x_{f_k} + \sum_{i=1}^{m}(\phi_f + \Gamma_f F_f C_f)^{m-i} \times (\Gamma_{fs} + \Gamma_f F_{fs})r_j + \left\{[(\phi_f + \Gamma_f F_f C_f) + (d\phi_f + d\Gamma_f F_f C_f)]^m - (\phi_f + \Gamma_f F_f C_f)^m\right\}x_{f_k} + \sum_{i=1}^{m}[(\phi_f + \Gamma_f F_f C_f) + (d\phi_f + d\Gamma_f F_f C_f)]^{m-i} \times [(\Gamma_{fs} + \Gamma_f F_{fs}) + (d\Gamma_{fs} + d\Gamma_f F_{fs})]r_j - \sum_{i=1}^{m}(\phi_f + \Gamma_f F_f C_f)^{m-i}(\Gamma_{fs} + \Gamma_f F_{fs})r_j \quad (28)$$

The slow controller defined by Eq. (18) is inserted into Eq. (28). Then, redefining the indices in terms of j (from the previous discussion $x_{f_k} = x_{s_j}, \ldots, x_{f_{k+m}} = x_{s_{j+1}}, \ldots$) and changing the subscript of x from f to s, we get

$$x_{s_{j+1}} = [(\phi_f + \Gamma_f F_f C_f)^m + \sum_{i=1}^{m}(\phi_f + \Gamma_f F_f C_f)^{m-i} \times (\Gamma_{fs} + \Gamma_f F_{fs})F_s C_s]x_{s_j} + \Bigg[\left\{[(\phi_f + \Gamma_f F_f C_f) + (d\phi_f + d\Gamma_f F_f C_f)]^m - (\phi_f + \Gamma_f F_f C_f)^m\right\} + \Bigg(\sum_{i=1}^{m}[(\phi_f + \Gamma_f F_f C_f) + (d\phi_f + d\Gamma_f F_f C_f)]^{m-i} \times [(\Gamma_{fs} + \Gamma_f F_{fs}) + (d\Gamma_{fs} + d\Gamma_f F_{fs})] - \sum_{i=1}^{m}(\phi_f + \Gamma_f F_f C_f)^{m-i}(\Gamma_{fs} + \Gamma_f F_{fs})\Bigg)(F_s C_s)\Bigg]x_{s_j} \quad (29)$$

or

$$x_{s_{j+1}} = (\hat{\phi} + \hat{\Gamma} F_s C_s)x_{s_j} + (d\hat{\phi} + d\hat{\Gamma} F_s C_s)x_{s_j} \quad (30)$$

where

$$\hat{\phi} = (\phi_f + \Gamma_f F_f C_f)^m \quad (31)$$

$$\hat{\Gamma} = \sum_{i=1}^{m}(\phi_f + \Gamma_f F_f C_f)^{m-i}(\Gamma_{fs} + \Gamma_f F_{fs}) \quad (32)$$

$$d\hat{\phi} = \left\{[(\phi_f + \Gamma_f F_f C_f) + (d\phi_f + d\Gamma_f F_f C_f)]^m - (\phi_f + \Gamma_f F_f C_f)^m\right\} \quad (33)$$

$$d\hat{\Gamma} = \sum_{i=1}^{m}[(\phi_f + \Gamma_f F_f C_f) + (d\phi_f + d\Gamma_f F_f C_f)]^{m-i} \times [(\Gamma_{fs} + \Gamma_f F_{fs}) + (d\Gamma_{fs} + d\Gamma_f F_{fs})] - \sum_{i=1}^{m}(\phi_f + \Gamma_f F_f C_f)^{m-i}(\Gamma_{fs} + \Gamma_f F_{fs}) \quad (34)$$

and where Eq. (30) represents the uncertain closed-loop system. Suppose that bounds are available on the maximum absolute values of the elements of dA and dB. That is,

$$|da_{ij}| \le (da_{ij})_{\max} \quad i = 1, \ldots, n, \qquad j = 1, \ldots, n \quad (35)$$

$$|db_{ij}| \le (db_{ij})_{\max} \quad i = 1, \ldots, n, \qquad j = 1, \ldots, m \quad (36)$$

Then, the corresponding bounds on the discrete model are given by

$$|d\varphi_f(i, j)| \le [d\varphi_f(i, j)]_{\max} \quad i = 1, \ldots, n, \qquad j = 1, \ldots, n \quad (37)$$

$$|d\gamma_f(i, j)| \le [d\gamma_f(i, j)]_{\max} \quad i = 1, \ldots, n, \qquad j = 1, \ldots, m \quad (38)$$

$$|d\gamma_{fs}(i, j)| \le [d\gamma_{fs}(i, j)]_{\max} \quad i = 1, \ldots, n, \qquad j = 1, \ldots, m \quad (39)$$

Define dA^+, dB^+, $d\phi_f^+$, $d\Gamma_f^+$, and $d\Gamma_{fs}^+$ as the matrices obtained by replacing the entries of dA, dB, $d\phi_f$, $d\Gamma_f$, and $d\Gamma_{fs}$ by their absolute values. Also define $A_{\max}$, $B_{\max}$, $\phi_{f,\max}$, $\Gamma_{f,\max}$, and $\Gamma_{fs,\max}$ as the matrices with entries $(da_{ij})_{\max}$, $(db_{ij})_{\max}$, $[d\varphi_f(i, j)]_{\max}$, $[d\gamma_f(i, j)]_{\max}$, and $[d\gamma_{fs}(i, j)]_{\max}$, respectively. Then,

$$\{dA: dA^+ \le A_{\max}\} \quad (40)$$

$$\{dB: dB^+ \le B_{\max}\} \quad (41)$$

The corresponding bounds in discrete time are

$$\{d\phi_f: d\phi_f^+ \le \phi_{f,\max}\} \quad (42)$$

$$\{d\Gamma_f: d\Gamma_f^+ \le \Gamma_{f,\max}\} \quad (43)$$

$$\{d\Gamma_{fs}: d\Gamma_{fs}^+ \le \Gamma_{fs,\max}\} \quad (44)$$

where

$$\phi_{f,\max} = \exp[(A^+ + A_{\max})T_f] - \exp(A^+ T_f) \quad (45)$$

$$\Gamma_{f,\max} = \int_0^{T_f} \exp[(A^+ + A_{\max})\tau]\,d\tau(B_f^+ + B_{f,\max}) - \int_0^{T_f} \exp(A^+\tau)\,d\tau B_f^+ \quad (46)$$

$$\Gamma_{fs,\max} = \int_0^{T_f} \exp[(A^+ + A_{\max})\tau]\,d\tau(B_s^+ + B_{s,\max}) - \int_0^{T_f} \exp(A^+\tau)\,d\tau B_s^+ \quad (47)$$

and where A^+, B_f^+, and B_s^+ are the matrices obtained by taking the absolute value of each element of A, B_f, and B_s, respectively. Here, $A_{\max}$, $B_{f,\max}$, and $B_{s,\max}$ are the matrices obtained by using the upper bound on the elements of dA, dB_f, and dB_s, respectively.

We now present the main theoretical result, which is a sufficient condition for robust stability of the multirate system in the presence of structured state space uncertainty.

Theorem 1. Suppose that F_f, F_{fs}, and F_s are such that the nominal closed-loop system described by Eq. (19) is asymptotically stable. Then, the uncertain closed-loop system given by Eq. (30) is asymptotically stable for all dA, dB_f, and dB_s that satisfy Eqs. (40–44) if

$$\lambda_{\max}\left\{\sum_{i=1}^{n}\frac{(v_i w_i^*)^+}{1-\xi_i^+}\psi_{c,\max}\right\} < 1 \tag{48}$$

where

$$\psi_c = \hat{\phi} + \hat{\Gamma} F_s C_s \tag{49}$$

The eigenvalues of ψ_c are ξ_i with v_i and w_i^* the corresponding right and left eigenvectors, respectively. Here $(\cdot)^*$ denotes the complex-conjugate transpose and $(\cdot)^+$ denotes absolute value. Also,

$$\psi_{c,\max} = \hat{\phi}_{\max} + \hat{\Gamma}_{\max}(F_s C_s)^+ \tag{50}$$

$$\hat{\phi}_{\max} = [(\phi_f + \Gamma_f F_f C_f)^+ + (\phi_{f,\max} + \Gamma_{f,\max}(F_f C_f)^+)]^m - [\phi_f + \Gamma_f F_f C_f)^+]^m \tag{51}$$

$$\hat{\Gamma}_{\max} = \sum_{i=1}^{m}[(\phi_f + \Gamma_f F_f C_f)^+ + (\phi_{f,\max} + \Gamma_{f,\max}(F_f C_f)^+)]^{m-i} \times [(\Gamma_{fs} + \Gamma_f F_{fs})^+ + (\Gamma_{fs,\max} + \Gamma_{f,\max} F_{fs}^+)] - \sum_{i=1}^{m}[(\phi_f + \Gamma_f F_f C_f)^+]^{m-i}(\Gamma_{fs} + \Gamma_f F_{fs})^+ \tag{52}$$

where $\phi_{f,\max}$, $\Gamma_{f,\max}$, and $\Gamma_{fs,\max}$ are given by Eqs. (45), (46), and (47), respectively.

Proof. The reader is referred to Ref. 8, which is the conference version of this paper.

Flight Control Design

We consider the lateral axis model of the L-1011 aircraft previously considered by Andry et al.[7] The model includes actuator dynamics and a washout filter on yaw rate. The states are rudder deflection δ_r, aileron deflection δ_a, bank angle ϕ, yaw rate r, roll rate p, sideslip angle β, and washout filter state x_7. The measurements are washed-out yaw rate r_{wo}, roll rate, sideslip angle, and bank angle. The control signals are rudder command δ_{rc} and aileron command δ_{ac}. The open-loop eigenvalues are $\lambda_{act} = -20$ for the rudder mode, $\lambda_{act} = -25$ for the aileron mode, $\lambda_{dr} = -0.0884 \pm j1.272$ for the dutch roll mode, $\lambda_{roll} = -1.085$ for the roll subsidence mode, $\lambda_{sp} = -0.00911$ for the spiral mode, and $\lambda_7 = -0.5$ for the washout filter mode. It is seen that the open-loop aircraft has a poorly damped dutch roll mode and the time responses in Ref. 7 show that the aircraft exhibits strong coupling from sideslip to bank angle.

First, an eigenstructure assignment stability augmentation inner loop controller is designed by using the augmented dynamics of Eq. (12) at a sampling rate of 50 Hz. The outputs available at the fast rate are washed-out yaw rate, roll rate, and sideslip angle. In addition, the outputs used for the gain computation also include the two uncontrollable states, which are due to the augmentation in Eq. (12). We remark that the eigenvectors that correspond to the dutch roll and roll subsidence modes lie in subspaces of dimension 2 whereas the eigenvectors that correspond to the uncontrollable modes lie in subspaces of dimension 4. A basis for these four-dimensional subspaces is obtained by using the MATLAB command "nullspace" on the matrix[9] $U_1^T(\lambda_{uc} I - A)$, where $\lambda_{uc} = 1$ and the singular value decomposition of the matrix B is given by

$$B = [U_0 \quad U_1]\begin{bmatrix}\Sigma V^T \\ 0\end{bmatrix} \tag{53}$$

The desired eigenvalues and eigenvectors of the matrix $\phi_f + \Gamma_f F_f C_f$ are shown in Table 1. The dutch roll mode is chosen to be well damped with a natural frequency of $\omega_n = 2.12$ rad/s and a damping ratio of $\zeta = 0.707$. The roll subsidence mode is chosen to have a time constant of 0.25 s in order to provide an adequate rise time. The other two modes, which are uncontrollable, correspond to the slow rudder and slow aileron. These modes arise from the augmentation of the $r_{k+1} = r_k$ equation to the fast dynamics in Eq. (12). The dutch roll eigenvector is chosen to be a yaw rate and sideslip mode with no coupling to roll rate and bank angle whereas the roll subsidence mode is chosen to be a roll rate mode with no coupling to yaw rate, sideslip, or the washout filter state. The slow rudder mode is chosen to include rudder and slow rudder with no coupling to the aileron and slow aileron whereas the slow aileron is chosen to include aileron and slow aileron with no coupling to the rudder or slow rudder.

The closed-loop eigenvalues and eigenvectors are shown in Table 2. The dutch roll and roll subsidence eigenvalues are achieved exactly because we have three aircraft outputs. The spiral mode, which cannot be assigned by the SAS, is at $s = 0.0029$. This small positive number is acceptable because the pilot who is flying the aircraft when the autopilot is off can easily compensate for this slow spiral motion. Furthermore, the time to double amplitude is within the specification for piloted vehicles.[10] If the pilot chooses not to keep his or her hands on the control stick or wheel, then the autopilot should be engaged. The boxed numbers in Table 2 indicate those eigenvector entries that were desired to be negligible. Observe that the dutch roll mode is characterized by coupling between yaw rate and sideslip with no coupling to roll rate or bank angle. The roll subsidence mode is characterized by roll rate and bank angle with very small coupling to yaw rate and sideslip. The spiral mode, which is not assigned by the SAS, is characterized by bank angle with small coupling to yaw rate and sideslip. Finally, the fast feedback gain F_f and the cross-coupling feedback gain F_{fs} are shown in Table 3.

Table 1 Desired eigenstructure for orthogonal projection design

SAS design					Autopilot design
Dutch roll		Roll subsidence	Slow rudder	Slow aileron	Spiral
$\lambda_{dr}^d = -1.5 \pm j1.5$		$\lambda_{roll}^d = -4$	(uncontrollable modes)		$\lambda_{sp}^d = -2$
$\begin{bmatrix}x\\x\\0\\1\\0\\x\\x\\x\end{bmatrix}$	$\pm j$ $\begin{bmatrix}x\\x\\0\\x\\0\\1\\x\\x\end{bmatrix}$	$\begin{bmatrix}x\\x\\x\\0\\1\\0\\0\\x\end{bmatrix}$	$\begin{bmatrix}1\\0\\x\\x\\x\\x\\x\\1\\0\end{bmatrix}$	$\begin{bmatrix}0\\1\\x\\x\\x\\x\\x\\0\\1\end{bmatrix}$ $\begin{matrix}\delta_r\\ \delta_a\\ \phi\\ r\\ p\\ \beta\\ x_7\\ \delta_r(\text{slow})\\ \delta_a(\text{slow})\end{matrix}$	$\begin{bmatrix}x\\x\\1\\x\\x\\0\\x\end{bmatrix}$ $\begin{matrix}\delta_r\\ \delta_a\\ \phi\\ r\\ p\\ \beta\\ x_7\end{matrix}$
Re v_{dr}^d	Im v_{dr}^d	v_{roll}^d	$v_{\delta_r}^d$ (slow)	$v_{\delta_a}^d$ (slow)	v_{sp}^d

Table 2 Closed-loop eigenstructure for orthogonal projection design[a]

Dutch roll	Roll subsidence	Spiral
Autopilot off		
$\lambda_{dr} = -1.5 \pm j1.5$	$\lambda_{roll} = -4$	$\lambda_{sp} = 0.0029$
$\begin{bmatrix} -0.7894 \\ -0.5775 \\ \boxed{0} \\ -0.1594 \\ \boxed{0} \\ 0.0056 \\ -0.0511 \\ 0 \\ 0 \end{bmatrix} \pm j \begin{bmatrix} -0.6139 \\ 0.4672 \\ \boxed{0} \\ -0.3276 \\ \boxed{0} \\ -0.1558 \\ 0.0872 \\ 0 \\ 0 \end{bmatrix}$	$\begin{bmatrix} 0.0441 \\ -1 \\ 0.0948 \\ \boxed{0.0003} \\ -0.3792 \\ \boxed{-0.0011} \\ 0 \\ 0 \\ 0 \end{bmatrix}$	$\begin{bmatrix} 0.0054 \\ 0.0015 \\ -1 \\ -0.0385 \\ -0.0029 \\ \boxed{-0.0013} \\ -0.0383 \\ 0 \\ 0 \end{bmatrix}$ $\begin{matrix} \delta_r \\ \delta_a \\ \phi \\ r \\ p \\ \beta \\ x_7 \\ \delta_r \text{ (slow)} \\ \delta_a \text{ (slow)} \end{matrix}$
Autopilot on		
$\lambda_{dr} = -1.5 \pm j1.5$	$\lambda_{roll} = -1.62$	$\lambda_{sp} = -2$
$\begin{bmatrix} -0.9989 \\ -0.2035 \\ \boxed{0} \\ -0.3189 \\ \boxed{0} \\ -0.0360 \\ 0.0084 \end{bmatrix} \pm j \begin{bmatrix} -0.0478 \\ 0.7145 \\ \boxed{0} \\ 0.1762 \\ 0 \\ 0.1652 \\ 0.1007 \end{bmatrix}$	$\begin{bmatrix} 0.1449 \\ -0.5035 \\ 0.6199 \\ \boxed{0.0466} \\ -1 \\ \boxed{0.0128} \\ -0.0209 \end{bmatrix}$	$\begin{bmatrix} -0.0937 \\ 0.8097 \\ -0.4999 \\ -0.0216 \\ 1 \\ \boxed{0} \\ 0.0072 \end{bmatrix}$ $\begin{matrix} \delta_r \\ \delta_a \\ \phi \\ r \\ p \\ \beta \\ x_7 \end{matrix}$

[a]The actuator, washout filter, and uncontrollable modes are not shown.

Table 3 Feedback gain matrices[a]

	F_f	F_{fs}	F_s
	r_{wo} p β	δ_{rcs} δ_{acs}	ϕ
Orthogonal projection	$\begin{bmatrix} 3.28 & -0.0726 & -4.70 \\ 1.43 & 2.14 & -6.30 \end{bmatrix}$ $\begin{matrix} \delta_{rcf} \\ \delta_{acf} \end{matrix}$	$\begin{bmatrix} -1.50 & -2.03 \\ -2.01 & -2.72 \end{bmatrix}$ $\begin{matrix} \delta_{rcf} \\ \delta_{acf} \end{matrix}$	$\begin{bmatrix} -1.62 \\ 0.474 \end{bmatrix}$ $\begin{matrix} \delta_{rcs} \\ \delta_{acs} \end{matrix}$
Robust multiobjective	$\begin{bmatrix} 3.57 & -0.194 & -5.32 \\ 1.58 & 2.31 & -6.69 \end{bmatrix}$	$\begin{bmatrix} -0.127 & -2.11 \\ -3.78 & -1.66 \end{bmatrix}$	$\begin{bmatrix} -0.580 \\ -0.0458 \end{bmatrix}$
Robust with gain suppression	$\begin{bmatrix} 3.35 & -0.191 & -4.87 \\ 1.43 & 2.17 & -6.32 \end{bmatrix}$	$\begin{bmatrix} 0 & -2.79 \\ -5.19 & 0 \end{bmatrix}$	$\begin{bmatrix} -0.398 \\ -0.0037 \end{bmatrix}$

[a]The symbols δ_{rcf}, δ_{rcs} represent the fast and slow rudder commands, respectively. The aileron symbols are defined similarly.

Next, we design the eigenstructure assignment autopilot outer loop, which operates at a rate of 10 Hz. The only output used for the autopilot design is bank angle. The eigenstructure assignment assigns the spiral mode of the matrix in brackets in Eq. (19). Of course, the other eigenvalues may shift, but if properly designed the final configuration will be acceptable. The desired spiral eigenvalue is chosen to yield a time constant of 0.5 s and the corresponding desired eigenvector is chosen to be a bank angle mode with no coupling to sideslip. A don't care entry is specified for yaw rate because bank angle should induce yaw rate to allow for a coordinated turn.

The closed-loop eigenvalues and eigenvectors for the system with the autopilot on are shown in Table 2. We observe that spiral has the desired time constant of 0.5 s and the dutch roll eigenvalues have not changed. The roll subsidence mode has moved to $s = -1.62$, which is acceptable even though it has a larger time constant than is the case with the autopilot off. The dutch roll eigenvectors exhibit the desired coupling to yaw rate and sideslip with no coupling to roll rate or bank angle. Although the roll subsidence eigenvalue has shifted, its corresponding eigenvector still exhibits the desirable characteristic of having bank angle dominant with small coupling to yaw rate and sideslip. The spiral eigenvector indicates that the desired roll rate and bank angle dominance is achieved with no coupling to sideslip. The slow feedback gain F_s is shown in Table 3.

Next, we use subroutine "attgoal" from the MATLAB Optimization Toolbox[11] to design a robust multirate eigenstructure assignment controller. The problem solved by "attgoal" is

$$\underset{p,\gamma}{\text{Minimize}}\ \gamma \qquad \text{subject to} \qquad F(p) - W\gamma \leq \text{goal} \tag{54}$$

where γ is used as a dummy argument to minimize the objectives $F(p)$.

The parameter vector p is chosen as follows: p_1 is the inner loop roll subsidence eigenvalue, p_2 the outer loop spiral eigenvalue, p_3 the inner loop dutch roll eigenvalue, (p_4, p_5, p_6, p_7) the inner loop dutch roll eigenvector parameters (which define a two-dimensional complex subspace), (p_8, p_9) the inner loop roll subsidence eigenvector parameters (which define a two-dimensional subspace), $(p_{10}, p_{11}, p_{12}, p_{13})$ the first uncontrollable mode eigenvector parameters (which define a four-dimensional subspace), $(p_{14}, p_{15}, p_{16}, p_{17})$ the second uncontrollable mode eigenvector parameters, and (p_{18}, p_{19}) the outer loop spiral eigenvector parameters (which define a two-dimensional subspace). The term *eigenvector parameters* is a vector z_i such that the ith eigenvector v_i is given by

$$v_i = L_i z_i \tag{55}$$

where L_i is a matrix whose columns form a basis for the subspace in which v_i must reside.

The objective functions are chosen as follows: f_1 is the robustness condition of Eq. (48) when the outer loop is closed (autopilot engaged), $f_2 = \|l^d_{dr} - l^a_{dr}\|^2$ is the inner loop dutch roll eigenvector projection error, $f_3 = \|l^d_{roll} - l^a_{roll}\|^2$ is the inner loop roll subsidence eigenvector projection error, $f_4 = \|l^d_{sp} - l^a_{sp}\|^2$ is the outer loop spiral eigenvector projection error, f_5 is the robustness condition of Eq. (48) when the outer loop is open (autopilot disengaged), $f_6 = f_7 = |p(3)|$, $f_8 = |p(3)| - \gamma_1$, and $f_9 = |p(3)| - \gamma_2$ where γ_1 and γ_2 are the discrete equivalents of damping ratios $\zeta_1 = 0.4$ and $\zeta_2 = 0.8$, respectively. The vectors l^d_i and l^a_i are the desired and

achievable specified components of the ith desired and achievable eigenvectors, respectively. These vectors are obtained, as shown by Andry et al.,[6] by defining a reordering operation $\{\cdot\}^{R_i}$ such that

$$\left\{v_i^d\right\}^{R_i} = \begin{bmatrix} l_i^d \\ d_i^d \end{bmatrix} \tag{56}$$

where l_i^d is a vector of specified components of v_i^d and d_i is a vector of unspecified components of v_i^d.

The objective f_5 cannot be computed directly because the spiral mode is unstable when the autopilot is not engaged. Therefore, we use a transformation[12] that decouples the spiral mode and yields a lower order model without the spiral. This transformation is applied to the matrices A, B, $A_{\max}$, and $B_{\max}$ and then this lower order model is discretized. This reduced-order model is only used to compute f_5 whereas the full-order model is used for all other computations.

The desired relationships between the objectives and the goals are chosen as follows: $f_1 \le 0.999$, $f_2 \le 0.01$, $f_3 \le 0.01$, $f_4 \le 0.01$, $f_5 \le 0.999$, $f_6 \le \exp(-T_f)$, $f_7 \ge \exp(-5T_f)$, $f_8 \le 1 \times 10^{-6}$, and $f_9 \ge 1 \times 10^{-6}$. These relationships define the vector "goal." The functions f_6 and f_7 constrain the dutch roll settling time by constraining $|\exp(\lambda_{\mathrm{dr}} T_f)|$ to the discrete equivalent of $\mathrm{Re}(\lambda_{\mathrm{dr}}) \in [-5, -1]$. The functions f_8 and f_9 constrain the dutch roll damping to the interval $\zeta_{\mathrm{dr}} \in [0.4, 0.8]$. To ensure the same percentage of under- or overattainment of the active objectives,[11] $w = \mathrm{abs(goal)}$ with the exception of goal(7) and goal(9), which are assigned minus signs because of the greater than or equal inequalities for f_7 and f_9. Hard constraints are placed on the settling times of the inner loop roll subsidence mode and the outer loop spiral mode. These constraints are given by $\exp(-6T_f) \le p_1 \le \exp(-2T_f)$ for the roll subsidence mode and $\exp(-3T_s) \le p_2 \le \exp(-T_s)$ for the spiral mode. This is equivalent to constraining the continuous-time eigenvalues to the intervals $\lambda_{\mathrm{roll}} \in [-6, -2]$ for the roll subsidence mode and $\lambda_{\mathrm{sp}} \in [-3, -1]$ for the spiral mode. The percentage uncertainties in the stability and control derivatives were chosen for illustrative purposes to be $\Delta Y_\beta = 15\%$, $\Delta L_\beta = 10\%$, $\Delta L_p = 25\%$, $\Delta L_r = 20\%$, $\Delta N_\beta = 30\%$, $\Delta N_p = 50\%$, $\Delta N_r = 15\%$, $\Delta Y_{\delta_r} = 15\%$, and $\Delta N_{\delta_a} = 20\%$.

The parameters p_i are initialized at the values from the orthogonal projection eigenstructure assignment design. The initial values of the objective vector is $F = (2.4127, 0.0000, 0.0000, 0.0000, 0.5125, 0.9704, 0.9704, -0.0165, 0.0097)^T$. We observe that the robustness condition f_1, which is for the case when the autopilot is engaged, is not satisfied. Also, we observe that the eigenvector projection errors f_2, f_3, and f_4 are zero to four decimal places. The optimal value of the objective vector is $F = (0.9781, 0.0098, 0.0056, 0.0099, 0.5047, 0.9673, 0.9673, -0.0196, 0.0067)^T$. We observe that both robustness conditions f_1 and f_5 are satisfied with f_1 being reduced by 60% from its initial value. However, this reduction in f_1 is achieved by allowing increases in the eigenvector projection errors, especially f_2 and f_4, which are close to their maximum goal values.

The optimal feedback gains are shown in Table 3, where we observe that the maximum cross-gain magnitude is larger and the slow gain magnitudes are smaller as compared with the orthogonal projection solution whereas the fast gains do not exhibit a significant change. The closed-loop eigenstructure is shown in Table 4, where we observe that the eigenvector entries, which were zero in the orthogonal projection design, are now nonzero. Thus, we expect that the coupling from sideslip to bank angle and from bank angle to washed-out yaw rate will be greater in the robust multiobjective design.

The SIMULINK multirate hybrid block diagram used to compute the time responses is shown in Ref. 8. Bank angle command following is achieved by feeding back the difference between bank angle and bank angle command. This approach results in zero steady-state error because of the type 1 characteristic of the bank angle subsystem. Also observe that the continuous aircraft inputs rudder command δ_{rc} and aileron command δ_{ac} are each the sum of two components. That is, rudder command is the sum of the output of the fast-rudder zero-order hold and the slow-rudder zero hold. The aileron command is similarly obtained.

The responses to a 1 deg initial sideslip angle when the autopilot is on are considered first. The solid curves indicate the orthogonal projection design whereas the dashed curves indicate the robust multiobjective design. The yaw rate and sideslip angle are shown in Fig. 2, where we observe that the speed and damping of the responses are excellent. Figure 3 shows the roll rate and bank angle where we observe the small coupling from sideslip to bank angle. Figure 4 shows the rudder and aileron deflections where we observe that the actuator deflection and deflection rates are similar to the continuous-time controller of Ref. 7.

Next, the responses to a 1 deg bank angle step command are considered. Figure 5 shows the bank angle and washed-out yaw rate responses where we observe that the goal of decoupling the yaw and roll channels has been achieved. In addition, the bank angle response exhibits acceptable rise time without overshoot.

The time responses are now considered for the case where the autopilot is turned off. Figure 6 shows the bank angle and roll rate for a 1 deg initial sideslip. We observe that the coupling to bank angle is again small, but as expected the bank angle does not return to zero. The very small divergence in the bank angle, which is caused by the unstable spiral, is easily compensated for by the pilot.

Finally, we compute a robust multiobjective design by using eigenstructure assignment with gain suppression,[7] which is embedded within the optimization. A design with two elements of F_{fs} suppressed to zero is shown in Table 3. These zero elements

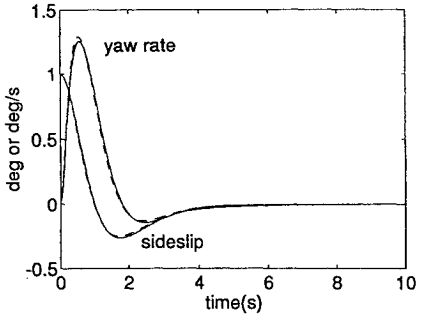

Fig. 2 Yaw rate and sideslip angle; $\beta(0) = 1$ deg, autopilot on.

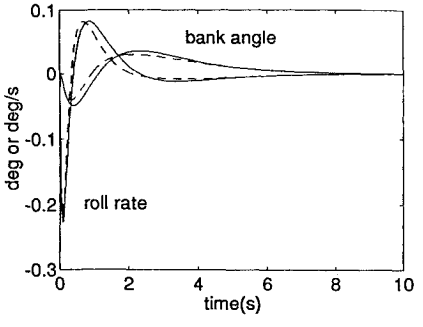

Fig. 3 Roll rate and bank angle; $\beta(0) = 1$ deg, autopilot on.

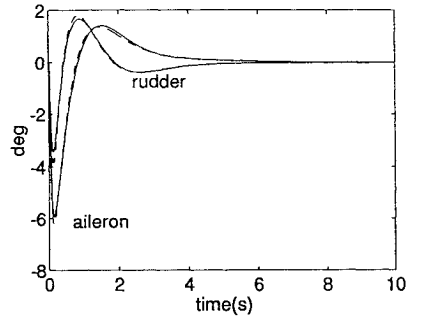

Fig. 4 Control deflections; $\beta(0) = 1$ deg, autopilot on.

Table 4 Closed-loop eigenstructure for robust multiobjective design[a]

Dutch roll	Roll subsidence	Spiral
Autopilot off		
$\lambda_{dr} = -1.66 \pm j1.51$	$\lambda_{roll} = -4.34$	$\lambda_{sp} = 0.0027$
$\begin{bmatrix} -1.000 \\ 0.1382 \\ \boxed{0.0010} \\ 0.1027 \\ \boxed{-0.0009} \\ 0.0151 \\ -0.0059 \\ 0 \\ 0 \end{bmatrix} \pm j \begin{bmatrix} \boxed{0.000} \\ -0.5130 \\ \boxed{-0.0008} \\ 0.0486 \\ \boxed{0.0003} \\ 0.0462 \\ -0.0287 \\ 0 \\ 0 \end{bmatrix}$	$\begin{bmatrix} -0.2336 \\ 1.000 \\ -0.0317 \\ \boxed{-0.0105} \\ 0.1429 \\ \boxed{-0.0017} \\ 0.0013 \\ 0 \\ 0 \end{bmatrix}$	$\begin{bmatrix} -0.0183 \\ -0.0025 \\ 1.000 \\ 0.0385 \\ 0.0028 \\ \boxed{0.0011} \\ 0.0383 \\ 0 \\ 0 \end{bmatrix}$ $\begin{matrix} \delta_r \\ \delta_a \\ \phi \\ r \\ p \\ \beta \\ x_7 \\ \delta_r \text{ (slow)} \\ \delta_a \text{ (slow)} \end{matrix}$
Autopilot on		
$\lambda_{dr} = -1.66 \pm j1.50$	$\lambda_{roll} = -2.88$	$\lambda_{sp} = -1.08$
$\begin{bmatrix} 1.000 \\ 0.1749 \\ \boxed{0.0066} \\ 0.3036 \\ -0.0042 \\ 0.0461 \\ -0.0180 \end{bmatrix} \pm j \begin{bmatrix} 0.0000 \\ -0.6051 \\ \boxed{-0.0045} \\ 0.1474 \\ \boxed{0.0175} \\ 0.1405 \\ -0.0871 \end{bmatrix}$	$\begin{bmatrix} -0.0595 \\ 1.000 \\ -0.2185 \\ -0.0054 \\ 0.6294 \\ \boxed{0.0016} \\ 0.0011 \end{bmatrix}$ $\begin{matrix} \delta_r \\ \delta_a \\ \phi \\ r \\ p \\ \beta \\ x_7 \end{matrix}$	$\begin{bmatrix} -0.0369 \\ -0.0085 \\ -0.9276 \\ \boxed{-0.0343} \\ 1.000 \\ \boxed{0.0030} \\ 0.0296 \end{bmatrix}$

[a]The actuator, washout filter, and uncontrollable modes are not shown.

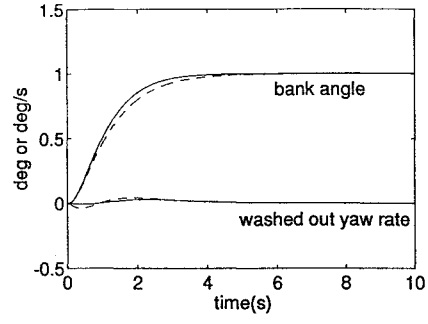

Fig. 5 Bank angle and washed-out yaw rate for ϕ command.

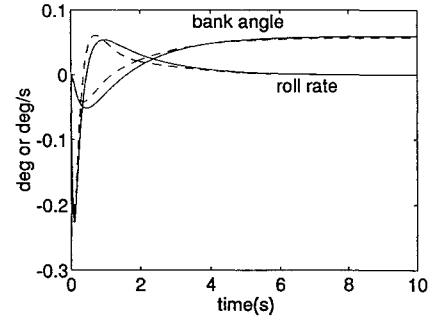

Fig. 6 Roll rate and bank angle; $\beta(0)$ = 1 deg, autopilot off.

represent the slow-rudder to fast-rudder and the slow-aileron to fast-aileron paths. The eigenvalues of this gain suppression design are insignificantly different from the full-gain design. The bank angle and washed-out yaw rate to a bank angle command are shown in Fig. 7. Here the solid line is the robust gain suppression controller and the dashed line is the robust full-gain controller. We observe that the responses are virtually identical even though the gain suppression controller has two gains eliminated from F_{fs}.

We remark that a robust gain suppression design with all four gains in F_{fs} suppressed to zero can be achieved. However, the spiral mode time constant of 4 s with the autopilot engaged was considered to be too large. Unfortunately, when elements of F_f were suppressed to zero, either the optimization did not converge to a stable solution

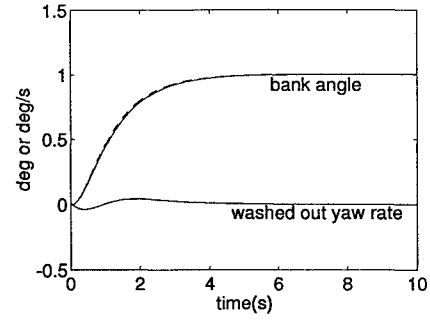

Fig. 7 Bank angle and washed-out yaw rate for ϕ command; gain suppression.

or the gains in F_{fs} became large, that is, gains with magnitudes in excess of 30.

Conclusions

A robust multirate eigenstructure assignment controller is designed for the lateral dynamics of the L-1011 aircraft at one flight condition by using a multirate structure with fast and slow loops. The design method uses a multiobjective optimization with both eigenstructure and robustness objectives. The stability augmentation system inner loop operates at 50 Hz and the bank angle autopilot outer loop operates at 10 Hz. The design exhibits excellent decoupling between an initial sideslip and bank angle. The bank angle command response is approximately first order with an excellent rise time and very small coupling to the washed-out yaw rate.

References

[1]Patel, Y., and Patton, R. J., "Insensitivity Properties of Multirate Feedback Control Systems," *Proceedings of the 30th IEEE Conference on Decision and Control* (Brighton, England, UK), Inst. of Electrical and Electronics Engineers, 1991, pp. 2954–2959.

[2]Araki, M., and Hagiwara, T., "Pole Assignment by Multirate Sampled Data Output Feedback," *International Journal of Control*, Vol. 44, No. 6, 1986, pp. 1661–1673.

[3]Patel, Y., Patton, R. J., and Burrows, S. P., "Design of Insensitive Multirate Aircraft Control Using Optimized Eigenstructure Assignment," *Journal of Guidance, Control, and Dynamics*, Vol. 16, No. 1, 1993, pp. 118–123.

[4]Huang, C. Y., "A New Approach to Analysis and Optimal Control Design for Multirate Control Systems," *Proceedings of the 1989 AIAA Guidance,*

Navigation, and Control Conference, AIAA, Washington, DC, 1989, pp. 602–607 (AIAA Paper 89-3496).

[5]Mason, G. S., and Berg, M. C., "Robustness Analysis of a Multirate Flutter Suppression System," *Journal of Guidance, Control, and Dynamics*, Vol. 16, No. 5, 1993, pp. 922–926.

[6]Piou, J. E., and Sobel, K. M., "Robust Sampled Data Eigenstructure Assignment Using the Delta Operator," *Journal of Guidance, Control, and Dynamics*, Vol. 16, No. 4, 1993, pp. 702–711.

[7]Andry, A. N., Shapiro, E. Y., and Chung, J. C., "Eigenstructure Assignment for Linear Systems," *IEEE Transactions on Aerospace and Electronic Systems*, Vol. AES-19, Sept. 1983, pp. 711–729.

[8]Piou, J. E., Sobel, K. M., and Shapiro, E. Y., "Robust Multirate Eigenstructure Assignment with Flight Control Application," *Proceedings of the AIAA Guidance, Navigation, and Control Conference* (Scottsdale, AZ), AIAA, Washington, DC, 1994, pp. 17–27 (AIAA Paper 94-3542).

[9]Kautsky, J., Nichols, N. K., and Van Dooren, P., "Robust Pole Assignment in Linear State Feedback," *International Journal of Control*, Vol. 41, 1985, pp. 1129–1155.

[10]Military Specification: Flying Qualities of Piloted Vehicles, MIL-F-8785C, U.S. Department of Defense, Nov. 5, 1980.

[11]Grace, A., *Optimization Toolbox for Use with MATLAB*™, Mathworks, Natick, MA, 1990.

[12]Stein, G., and Henke, A. H., "A Design Procedure and Handling Quality Criteria for Lateral Directional Flight Control Systems," Air Force Flight Dynamics Laboratory, AFFDL-TR-70-152, Wright-Patterson AFB, OH, May 1971.